Improvement of the wear resistance of nickel-aluminium bronze and 2014-T6 aluminium alloy by application of alternating magnetic field treatment

Sufyan Akram[1], Anatolii Babutskyi[1,2], Andreas Chrysanthou[1], Diogo Montalvão[3], Mark J. Whiting[4], Nada Pizurova[5]

[1] School of Physics, Engineering and Computer Science, University of Hertfordshire, Hatfield, AL109AB, United Kingdom (a.babutskyi@herts.ac.uk / s.akram3@herts.ac.uk / a.chrysanthou@herts.ac.uk)

[2] G.S. Pysarenko Institute for Problems of Strength, National Academy of Sciences of Ukraine, Kyiv, 01014, Ukraine

[3] Department of Design and Engineering, Faculty of Science and Technology, Bournemouth University, Poole House, Talbot Campus, Fern Barrow, Poole BH12 5BB, United Kingdom (dmontalvao@bournemouth.ac.uk)

[4] Department of Mechanical Engineering Sciences, University of Surrey, Guildford, Surrey GU2 7XH, United Kingdom (m.whiting@surrey.ac.uk)

[5] Institute of Physics of Materials, Academy of Sciences of the Czech Republic, v.v.i., Žižkova 22, CZ61662 Brno, Czech Republic (pizurova@ipm.cz)

Abstract

The present work has used an alternating magnetic field treatment at ambient temperature to improve the wear resistance of nickel-aluminium bronze and aluminium alloy 2014-T6. Pin-on-disc wear tests under lubricating conditions using a AISI52100 steel ball bearing as the counter face material have shown reduction in the width and depth of wear scars as well as lower values of the coefficient of friction following the treatment. The improved wear properties have been attributed to increased precipitation of κ_{IV} in the case of the nickel-aluminium bronze and of GP zones as well as θ'' for AA2014-T6. Transmission electron microscopy also revealed changes in the dislocation distribution, while X-ray diffraction showed changes in the residual stress for both alloys. The mechanism leading to these changes is discussed by consideration of the soft ferromagnetic properties of the nickel-aluminium bronze and the paramagnetic nature of AA2014.

Magnetic field treatment, nickel-aluminium bronze, aluminium, precipitation hardening

1. Introduction

Controlling friction and reducing wear using advanced tribological technology can save resources, prolong service life and increase reliability in wear-critical applications [1]. There are two general approaches that can be used to reduce wear; these are based on reducing friction through the use of liquid or solid lubricants between working faces or by modifying the materials and their properties. The external parameters that are used to process materials for improvement in their properties are pressure, temperature and time. A relatively new research field is beginning to emerge investigating the use of external fields (like magnetic fields) to process solid-state materials. For example, Bockstedt et al. [2] have reported that pulsed magnetic field treatment can lead to changes in the hardness and in the state of residual stresses (RS) in materials, while a study by Bataineh et al. [3] has shown benefits in reducing the wear of cutting tools. In the latter investigation [3], tests for high-speed steel drills that had undergone pulsed magnetic field treatment were reported to result in an increase in the number of drilled holes by about 15% compared to drills in the untreated condition. In another study conducted by Babtuskyi et al. [4] it was demonstrated that the application of pulsed magnetic field treatment to AISI 52100 steel led to a reduction in the sliding friction properties by 13%. Similar findings have been reported by Xi, Xia [5] who studied the effect of pulsed magnetic field treatment on the tribological behaviour of AISI 1045 steel and reported reduction in the size of wear tracks and in the value of the coefficient of friction as a result. In spite of recent interest in the use of magnetic fields to process materials, the effect of exposure to a magnetic field on the tribological behaviour of

metals is not well-understood and the mechanisms that might lead to improvement in behaviour are unclear.

The main objective of this work was to investigate the effect of alternating magnetic field treatment on the wear and frictional properties of nickel aluminium bronze (NAB) and aluminium AA2014-T6. While recent research has addressed the use of pulsed magnetic field treatment, the number of studies making use of alternating magnetic field treatment is rather limited. Alternating magnetic field treatment has the advantage of being easier and safer to operate and uses simpler and more cost-effective equipment in comparison to pulsed magnetic field treatment. The pin-on-disc test has been selected specifically because NAB are used as deep-drawing tooling [6] and AA2014-T6 can be used as automotive bearing caps in contact with hard steel with oil as a lubricant [7]. Specimens were magnetically treated and tested using pin-on-disc tests. For the analysis of the effects of the treatment, RS measurements were carried out by using X-ray diffraction (XRD) for both treated and untreated conditions, while microstructural changes were examined using scanning electron microscopy (SEM) as well as transmission electron microscopy (TEM).

2. Experimental Methodology

Cold-rolled nickel-aluminium bronze (NAB) NES833 DEF-STAN 02-833 and extruded aluminium 2014 in the T6 temper condition (AA2014-T6) were used in this investigation. The normal compositions of NAB are as follow (wt.%): Al, 8.5 − 10; Ni, 4 − 5; Fe, 4 − 5; Mn, 0.5; Cu, balance and the normal compositions of AA204-T6 are as follow (wt.%): Si, 0.5 − 1.2; Fe, 0.7; Cu, 3.9 − 5; Mn,0.4 − 1.2; Mg, 0.2 − 0.8; Cr, 0.1; Zn, 0.25; Ti, 0.15; Other, 0.15.

NAB bar of 25.4 mm diameter and AA2014-T6 bar of 26 mm diameter were sliced to a thickness of 2.9 mm by using a Struers Secotom-10 cutting machine at a very low feed rate and using water as a coolant. Prior to testing, the samples had been ground and finely polished using a 0.3 μm diamond suspension. The test parameters were set in accordance with the ASTM 99-95a Pin-on-disc standard [8]. The disc samples were tested under sliding conditions using a POD 2 pin-on-disc tester (Teer Coatings Ltd.). Both alloys were tested by using a linear velocity of 50 mm/s for 60 min at an ambient temperature of 22°C. Sunflower oil used used as a lubricant; vegetable oils have been used in many tribological studies as lubricants because they are sustainable and friendly to the environment, while recent studies [9] have demonstrated superior performance over conventional oils. AISI52100 contact ball bearings of 5 mm diameter were used as the counter face material. The ball bearings had a Rockwell hardness (HRC) of 62–64 and surface roughness (R_a) of 20 nm. A vertical load of 6 N was applied for AA2014-T6 and 10 N for NAB. The experimental parameters for the pin-on-disc tests are presented in Table 1. These values were chosen in order to achieve accelerated wear of the samples for quick comparison between treated and untreated samples. The pin-on-disc samples were cleaned thoroughly with acetone prior to each test. A precision digital scale with an accuracy of ± 0.1 mg was used to weigh the samples before and after each pin-on-disc test. The specific wear rate for the tested materials was obtained by using the equation below:

$$W = \frac{\Delta w}{L \rho F}$$

Table 1. Pin-on-disc test parameters.

	Rotational speed, RPM	Load, N	Track diameter, mm	Testing time, s	Linear velocity, mm/s
NAB	80	10	12	3600	50
AA2014-T6	80	6	12	3600	50

where W is the specific wear rate in mm³/Nm, Δw is the weight loss measured in grams, L is the sliding distance in m, ρ is the density of the worn material in g/mm³ and F is the applied load in N. The same specimen geometry was used also for X-ray diffraction (XRD), microhardness testing, electrical conductivity measurements and magnetic force microscopy (MFM).

Alternating magnetic field treatment of duration of 30 minutes was performed by placing the samples in a magnetiser. Figure 1a displays the magnetic field direction during the treatment of samples, while Figure 1b presents the registration of the magnetic field without the presence of any specimen in the magnetiser. The magnetic field recorded in the absence of any sample was 1.24 T. The same magnetiser settings were used for the processing of both metals. The magnetic flux density was measured by using a Hirst GM08 Gaussmeter. The registration of the magnetic flux density was conducted by using a digital oscilloscope (Picoscope 4224). A K-type thermocouple was used to measure the temperature of the sample during the treatment. The recorded temperature increase was 10.5°C for the NAB sample and 10.8 °C for AA2014-T6.

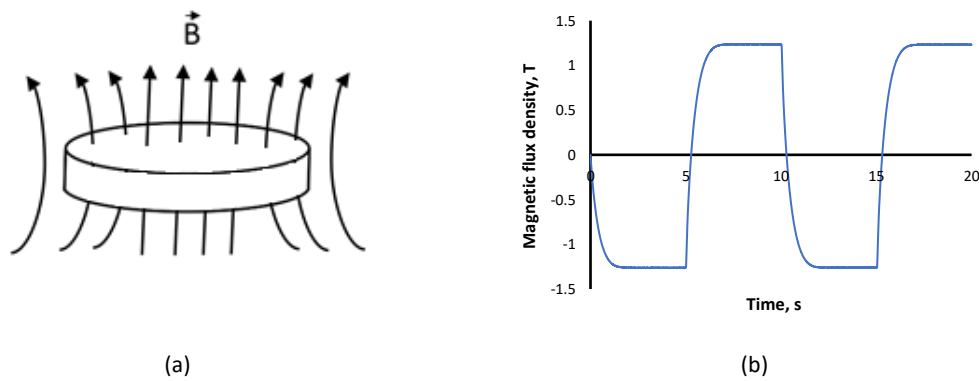(a)   (b)

Figure 1. Schematic showing the direction of the applied alternating magnetic field for the disc samples (a) and the magnetic flux density during treatment (b).

Microhardness testing was performed using a Struers DuraScan 20 microhardness tester at a load of 1 N. The microhardness values that are presented in this work were the average values of 60 measurements across two radii for each sample. Morphological observations of the wear scar width for both treated and untreated samples were carried out using a JEOL JSM-5700F scanning electron microscope (SEM) operated at 20 kV. The surface profile and the average surface roughness measurements of the wear tracks were performed by employing a Mitutoyo Surftest SJ-500 2D surface profiler with a stylus tip radius of 2 μm and and angle of 60°. Considering the fact that measurements of electrical conductivity can provide valuable data regarding precipitation in AA2014-T6 aluminium alloy [10-14], this property was measured at room temperature before and after treatment by using a Foerster SIGMA TEST 2.069 conductivity meter.

MFM was conducted by using an Easyscan 2 Atomic Force Microscope (AFM) made by Nanosurf in order to detect any changes in the magnetic domains within the magnetically treated and untreated NAB alloy. Using a Neodynium magnet MagneticMulti74-G cantilever probe, the scanning range was set to 10 μm by 10 μm and the probe height was 60nm.

Phase identification and RS measurements were performed with a Bruker D8 Advance X-ray diffractometer using Cu-K$_\alpha$ radiation of wavelength 1.540549 Å and radiation energy of 8.05 keV. The XRD tube voltage and current were set at 40 kV and 40 mA respectively. The peaks evaluated for NAB and AA 2014 -T6 were 2θ = 115° (4 0 0) and 2θ = 116.6° (4 2 2) respectively. For calculating RS, the Sliding Gravity method was used as it is the preferred method for measuring RS for industrial products [15]. Furthermore, background subtraction, smoothening, K$_{\alpha 2}$ correction, absorption correction and

polarization corrections were applied to improve the accuracy of the results. The stress model calculated was based on normal stress using the Bruker Leptos software version 7.9.

Transmission electron microscopy (TEM) was preformed by using a JEOL JEM-1400F operating at an accelerating voltage of 120 kV. Both alloys were examined in the magnetically treated and untreated condition. Additional TEM analysis using a Titan Themis 60-300 cubed with an accelerating voltage of 300 kV was employed to study the precipitates present in the AA2014-T6 material. Electron transparent foil samples were prepared using standard mechanical thinning and electropolishing techniques. The samples for the TEM examination were prepared from foils by sectioning from the near-surface area of the magnetically treated and untreated samples.

3. Results

The results of the pin-on-disc tests for treated and untreated NAB and AA 2014-T6 are presented in Figure 2a and Figure 2b. Figure 2a shows that the treated NAB sample retained a lower coefficient of friction for a longer period of time than the untreated sample did (about twice as much). During the run-in stage, the coefficient of friction for the treated sample was 0.37 compared to a value of 0.44 for the untreated NAB (a 16% decrease). Figure 2b shows that in the case of AA2014-T6 the treated sample retained almost a constant coefficient of friction of about 0.13 for about 30 minutes, while the value for the untreated sample saw significant and progressive increase from the start of the test. The specific wear rate for the treated AA2014-T6 and NAB (as shown in Figure 2c) decreased by 56% and 61% respectively in comparison to the untreated condition.
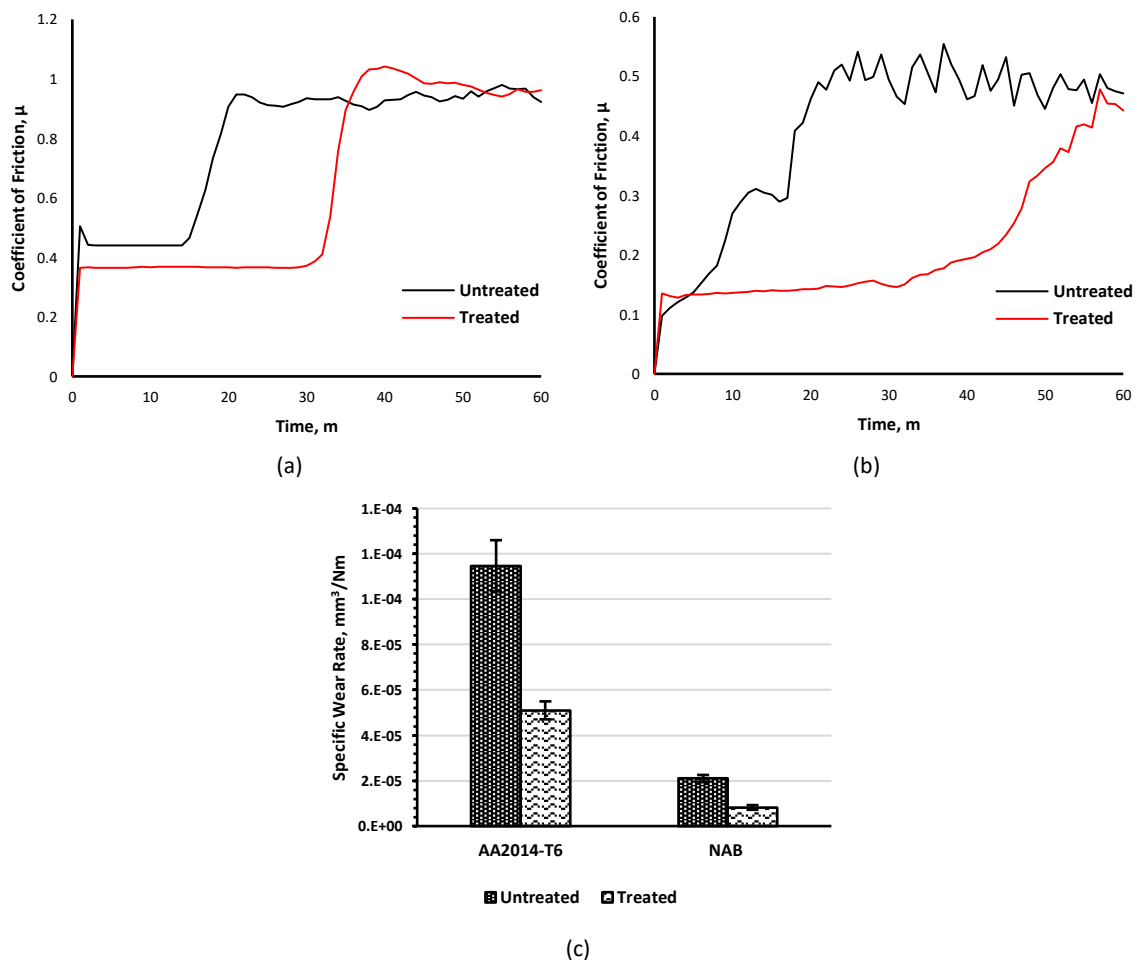

(a)

(b)

(c)

Figure 2. Variation of the coefficient of friction for treated and untreated NAB (a), AA2014-T6 specimens (b) and the specific wear rates of treated and untreated NAB and AA2014-T6 samples (c).
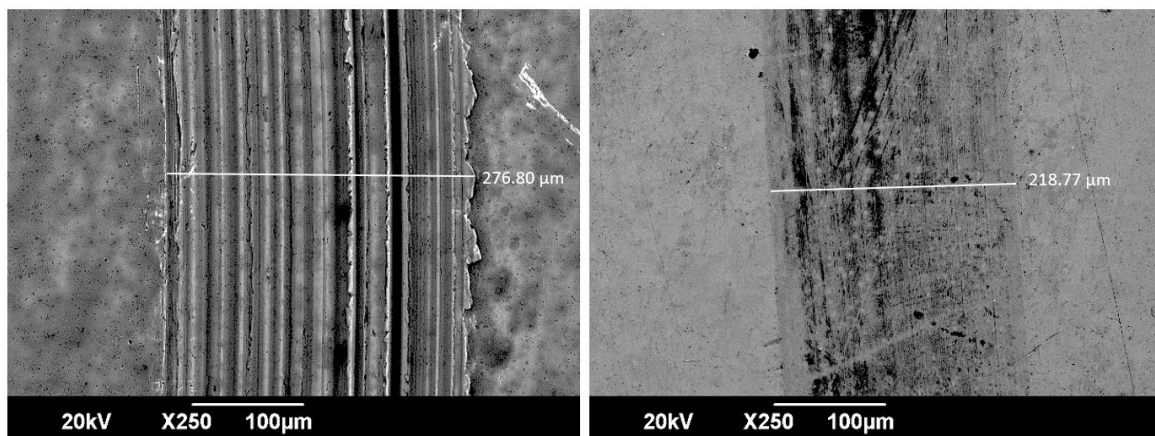
The results for microhardness, average wear scar width, surface roughness of the wear track, electrical conductivity and RS are summarised in Table 2. The RS data show that following treatment, the NAB samples had experienced a drop in the tensile RS by approximately 40%. In the case of AA2014-T6, the untreated sample exhibited tensile RS which became compressive following treatment with the alternating magnetic field. In addition, there was a reduction in the wear scar width of 18% and 15% for NAB and AA 2014-T6 respectively. Furthermore, the average surface roughness of the wear track decreased by 20% for NAB and 44% for AA2014-T6 following the treatment. Electrical conductivity measurements for the AA2014-T6 alloy showed a 0.9% reduction from 22.99 MS/m in the initial condition to 22.77 MS/m after treatment with corresponding mean-square deviation values of 0.039 MS/m and 0.033 MS/m respectively (based on measurements using 3 samples with 20 measurements per sample).

Table 2. Mean (M) and mean-square deviation (MSD) results of microhardness (Vickers), RS, wear track width and surface roughness of wear tracks R_a.

Sample condition		Microhardness[1], HV		RS[2], MPa		Wear scar width[3], µm		Surface roughness of wear tracks R_a[4], µm	
		M	MSD	M	MSD	M	MSD	M	MSD
NAB	Untreated	142.2	5.7	39.6	116.7	272.5	8.8	0.201	0.019
	Treated	151.1	2.7	23.7	107.1	222.8	6.0	0.159	0.013
AA2014-T6	Untreated	221.8	19.7	59.0	36.9	517.5	7.0	0.580	0.026
	Treated	231.8	23.8	-12.0	23.3	439.7	10.5	0.326	0.008
[1] average of 60 indentations per sample (3 samples); [2] average of 3 samples; [4] average of 4 measurements per sample (one measurement in every quadrant, 3 samples); [3] average of 5 measurements per sample (3 samples).									

Figure 3a-d show SEM micrographs of the worn surfaces of the treated and untreated NAB and AA2014-T6 respectively. According to the evidence, the NAB and AA2014-T6 untreated samples revealed several deep grooves as well as pits on their surface. In contrast to the untreated samples, the grooves and pits that were observed for the AFM-treated NAB and AA2014-T6 samples were relatively shallow. Support for this observation was provided by the results in Figure 4 which shows a comparison of 2D surface profiles of the wear tracks for the treated and untreated NAB (Figure 4a) and AA2014-T6 (Figure 4b). The results indicate that the depth of the wear tracks produced for the untreated condition for both alloys was greater and wider than for the samples in the treated condition. In addition, bulging on both sides of the wear tracks was more prominent in the untreated case as opposed to the treated condition for AA2014-T6. Furthermore, the evidence in Figure 4b shows more advanced stages of pull-out wear for AA2014-T6 in the untreated condition. Bulging was also apparent at the surface of the NAB untreated specimen, but in this case the effect was slightly less compared to the NAB sample.

(a)   (b)

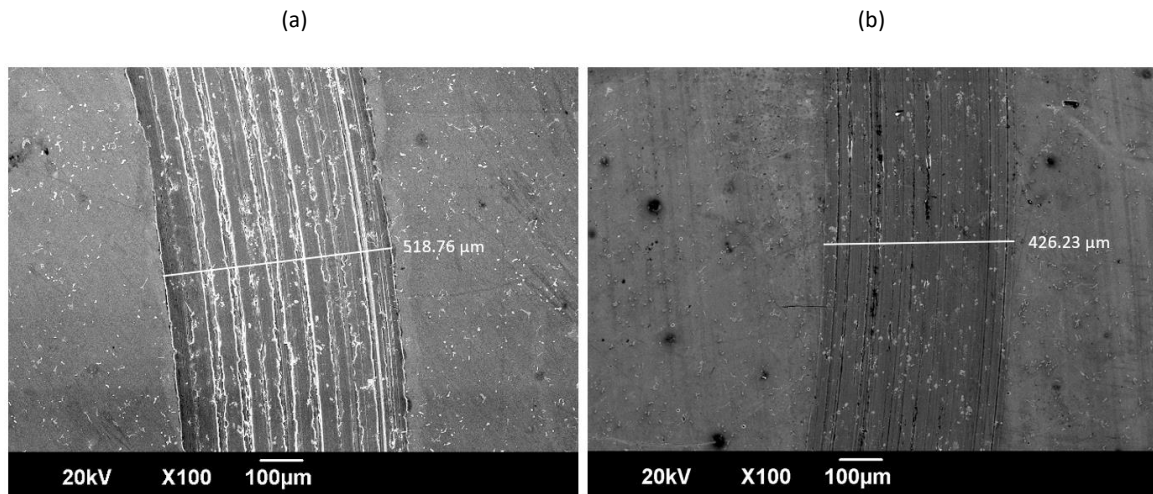(c)   (d)
Figure 3. SEM of wear tracks of the surface of untreated (a) and treated NAB (b) after 1 hour and untreated (c) and treated AA2014-T6 (d) after 1 hour.
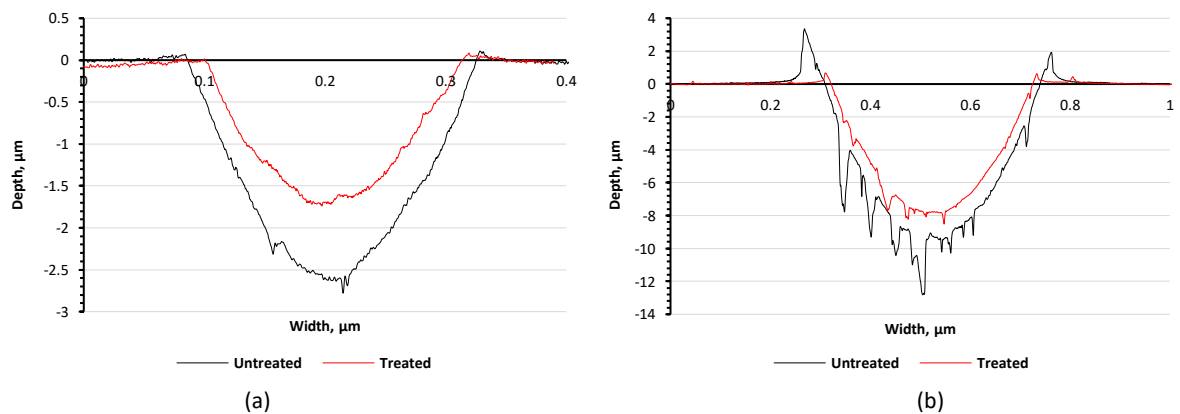

(a)   (b)
Figure 4. Comparison of 2D surface profile of Untreated (black) and treated (red) NAB (a) and AA2014-T6 (b).

(a)   (b)
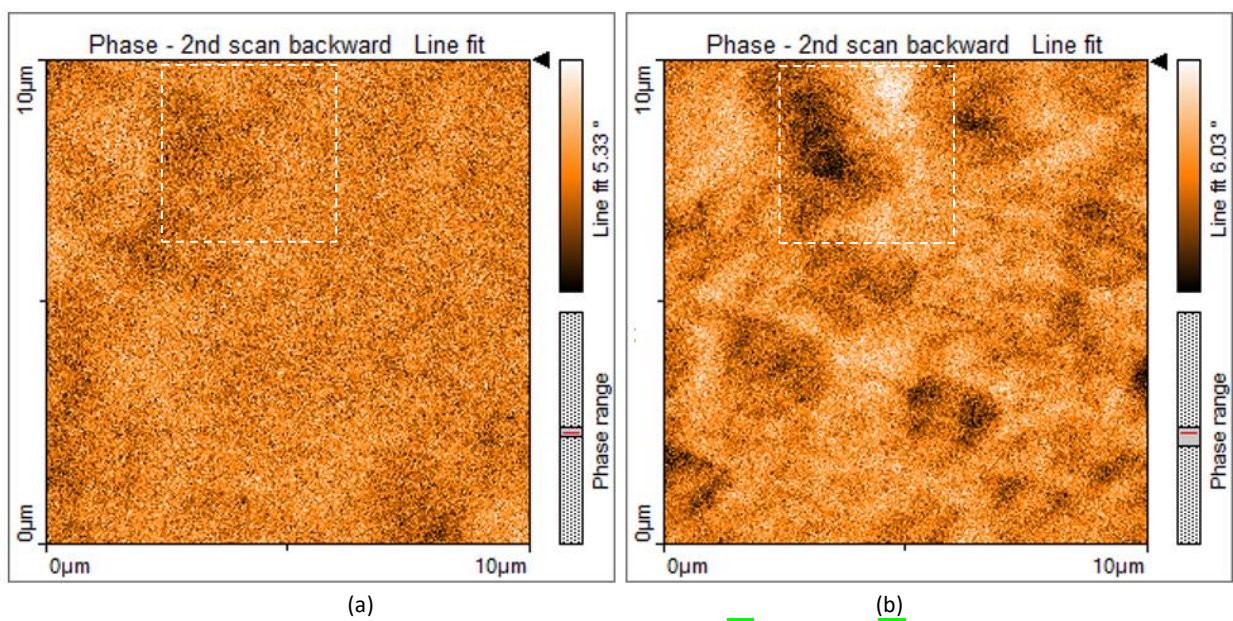Figure 5. Magnetic domain structure of untreated (a) and treated (b) NAB.

Figure 5 presents the magnetic domain structure of the same area of a NAB sample prior to and following alternating magnetic field treatment. The MFM images indicate the degree of deviation of the magnetisation vector direction from the orientation direction of the sample . The regions of dark contrast represent areas where an attractive magnetic force gradient occurs (this is the result of the resonance curve shifting to a lower frequency). On the other hand, at the areas of bright contrast there is a repulsive magnetic force gradient. Some transition regions also occur; these are regions where the magnetic moment direction deviates from the magnetisation axis. The magnetic domain structure seems to change after the application of the alternating magnetic field. The treated NAB appears to exhibit larger and more defined areas of an attractive magnetic force gradient in contrast to a more random situation in the untreated sample. These observations suggest that following treatment there appears to be more magnetisation of the domains within the material. Figure 6 displays XRD phase analysis for NAB in both the treated and untreated states. The XRD results revealed that due to the treatment there is a slight rearrangement in the β phase and a slight increase in the copper-rich α phase.
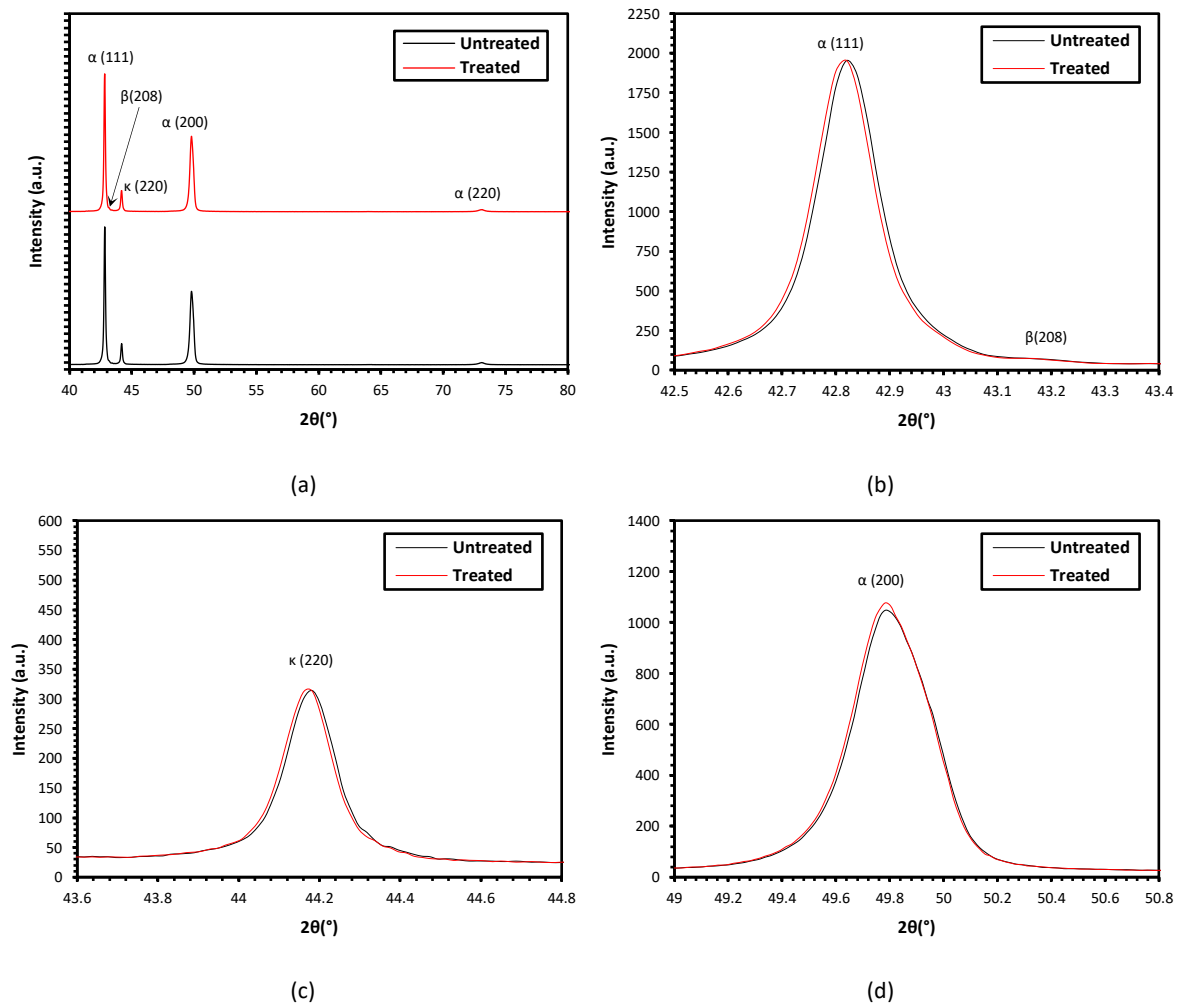

(a)

(b)

(c)

(d)

Figure 6. XRD pattern NAB and diffraction peak profiles of untreated (black) and AMF treated (red) samples XRD patterns (a), (111) diffraction peak (b), (220) diffraction peak (c) and (200) diffraction peak (d).

Typical bright field TEM micrographs of the treated and untreated NAB are shown in Figure 7. Figure 7a presents a typical area exhibiting a relatively high dislocation density, where dislocation tangles, pile-ups and stacking faults are evident. According to the evidence shown in Figure 7b, the application of the alternating magnetic field treatment has led to fewer dislocation pile-ups at the

grain boundaries, fewer stacking faults and reduced entanglement of dislocations. The observation of a lower dislocation density implies that annihilation of dislocations has taken place as a result of the treatment. In addition, Figure 7b shows the emergence of more fine κ_{IV} spherical precipitates following alternating magnetic field treatment.
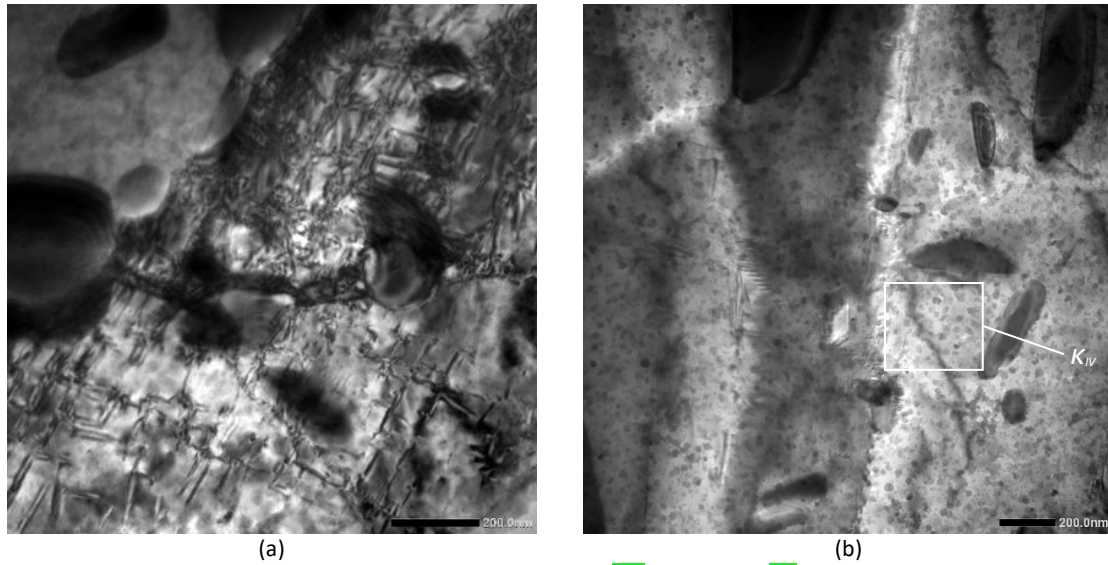

Figure 7. TEM images of untreated (a), and treated (b) NAB.

Figure 8 shows bright-field TEM images of AA2014-T6 before and after alternating magnetic field treatment. The image for the untreated material in Figure 8a shows evidence of relatively high dislocation density pile-ups, while Figure 8b suggests that the treated sample exhibited fewer dislocation pile-ups in comparison. Furthermore, a higher density of uniformly distributed, fine needle-shaped precipitates is present in the sample in the treated condition. TEM mapping as displayed in Figure 9 reveals a morphology consistent with the presence of GP zones and θ'' precipitates as as a result of the application of an alternating mangetic field as demonstrated recently by Akram, Babutskyi [16]. The presence of these strengthening precipitates is further supported by the decrease in the electrical conductivity of AA2014-T6 following the treatment.
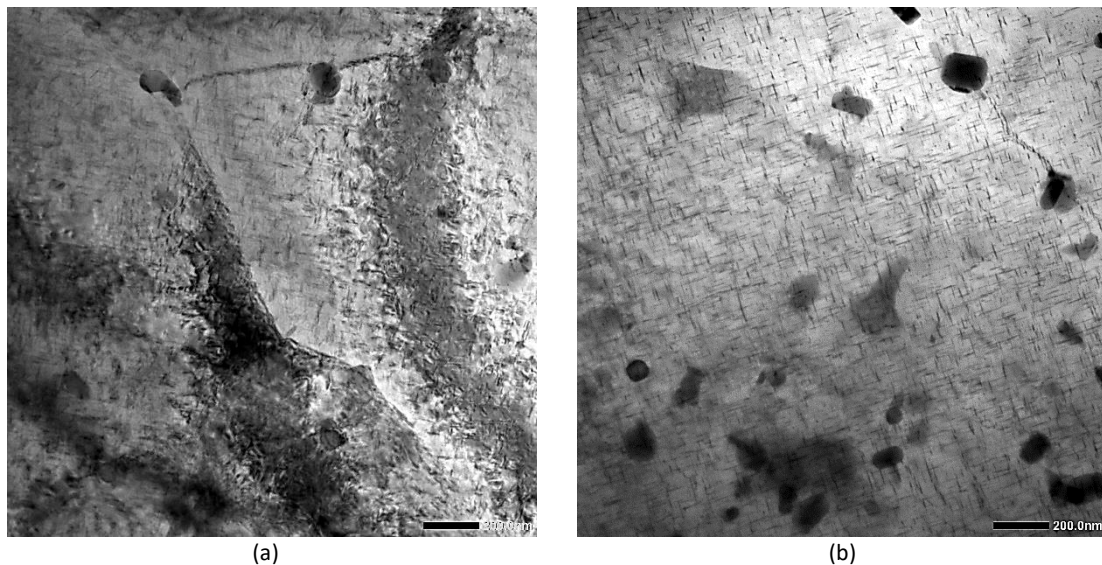

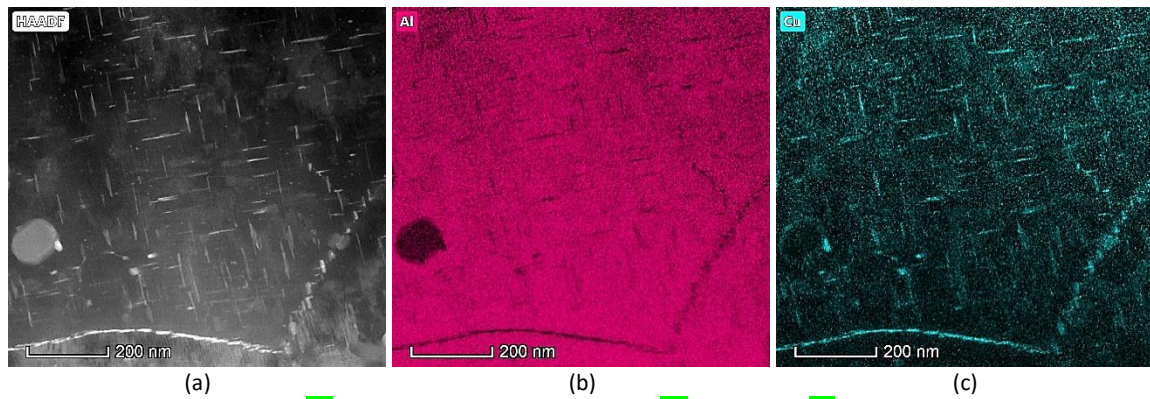Figure 8. TEM images of untreated (a) and treated (b) AA2014-T6.

Figure 9. TEM image (a) and TEM mapping of aluminium (b) and copper (c) in treated AA2014-T6.

4. Discussion

The results for the specific wear rates and the wear track measurements have demonstrated that there was an improvement in the wear resistance of both NAB and 2014-T6 alloy as a result of alternating magnetic field treatment. The XRD data have shown a decrease in tensile RS in the near-surface layer of NAB and the presence of compressive RS for the aluminium alloy following the treatment. The TEM investigation has determined that there was a reduction in the pile-up of dislocations in the AA2014-T6 sample after treatment, while the generation of more strengthening precipitates was also apparent. The TEM observations for the NAB alloy showed more uniform dislocation distribution after treatment, while a substantially higher amount of the κ_{IV} phase (the main contributor to NAB strengthening) was detected. There is also evidence that the microhardness of the AA2014-T6 and NAB alloys increased as a result of the application of the alternating magnetic field treatment. The lower standard deviation for the microhardness results following treatment suggests that in both cases, the treatment had led to a more homogeneous microstructure. This type of homogenisation of the microstructure, together with reduced tensile RS at the surface of the sample creates conditions to reduce friction and wear. Dislocation movement is normally activated thermally; however, the measured increase in temperature during the treatment of both alloys was very low (about 10 - 11°C) and such rise is not sufficiently high to promote any notable changes in microstructure and properties. It is therefore likely that these effects were activated athermally. This observation was in support of previous research by Tang et al. [17] who reported that the application of a pulsed magnetic field had brought about changes in the mechanical properties of 30CrMnSi high-strength steel through an athermal mechanism. In order to understand the driving mechanisms that lead to microstructural and property changes through the use of an alternating magnetic field, it is important to consider the nature of the two alloys; for example, NAB has soft ferromagnetic properties due to its composition (which contains iron and nickel), while AA2014-T6 alloy is paramagnetic. In addition, there must be consideration of the applied parameters of the external field. In the current work, the magnetic flux density that was applied between the two magnetic poles was 1.24 T; the AA2014-T6 samples were thus exposed to a magnetic flux density of 1.24 T because this alloy has relative permeability, μ_{AA2014}, of 1. However, the NAB samples encountered a higher magnetic flux density, as this bronze has relative permeability, μ_{NAB}, of 1.5 [6] and it is magnetised under an external magnetic field; therefore the total magnetic flux density to which the NAB alloy was exposed was higher in comparison to that for AA2014-T6. In addition, there must be consideration of the fact that the stepwise change of the magnetic field polarity had induced eddy currents into the samples. In total, the change of the magnetic flux density was 2.48 T every 5 seconds. During each polarity change, pulsed eddy currents were induced and therefore the samples were exposed to not only an alternating magnetic field but also to a periodic pulsed electric current.

The distribution of the eddy currents and the magnetic field were estimated by means of finite element analysis and numerical modelling using QuickField 6 software. For the solution of this transient magnetic field problem, a 2D formulation was applied. The geometrical model that was used

for the calculations was based on the dimensions of the magnetiser and the samples (Figure 10). The physical properties that were used for the modelling are presented in Table 3.

Table 3. Physical properties of materials used during modelling.

Property	Core (steel)	Spacer (steel)	Winding wire (copper)	NAB sample	AA2014-T6 sample	Air
Electrical conductivity, MS/m	10	10	56	2.3	23	0
Relative permeability	B-H curve*	B-H curve*	1	1.5	1	1

*The magnetic flux density vs magnetic field strength (B-H) curve for steel was taken from [18].

The full current time variation $I(t)$, that passes through a turn of the magnetiser windings can be presented in the form of a sign function:

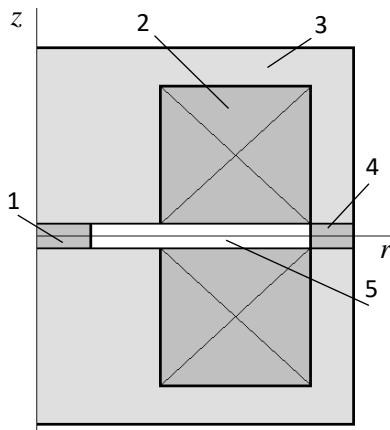$$I(t) = I_0 \, sign \, (sin \, (2\pi t/T)),$$

Figure 10. Scheme of axisymmetric model used at numetical modelling: 1 – disc sample, 2 – winding; 3 – magnetiser core; 4 – 3 mm steel spacer, 5 – air, z – axis; r – radius.

where T is the period within which the field in the magnetiser acts in both directions (10 s, refer to Figure 1b). The value of I_0 was determined from the best fitting of the registered and calculated profiles of the magnetic field for the magnetiser without a sample; the value obtained was 1.24 T (Figure 1b). Numerical modelling was fulfilled for the magnetizer with (i) AA2014-T6 and (ii) NAB samples located at the centre of the magnetiser as presented in Figure 10 with an axisymmetric model of the treatment arrangement.

According to the numerical modelling results, the NAB samples were exposed to a magnetic flux density of around 1.8 T (due to its relative permeability of 1.5). The change of the polarity of the magnetic field (see Figure 1b) causes maximum eddy currents of 1.26×10^6 A/m^2 and 9.2×10^6 A/m^2 for NAB and AA2014-T6 respectively (see Figure 11); these maximum values were reached at the cylindrical surface of the samples. A number of researchers including Baranov et al. [19] and Stepanov et al. [20] have observed the relaxation of RS in metals as a result of the application of a pulsed electric current. According to Baranov et al. [19], notable changes in the mechanical properties and relaxation as well as redistribution of RS occur when the electric current density exceeds a threshold level of about 1×10^8 to 1×10^9 A/m^2. Following on from this, Stepanov et al. [20] observed relaxation of RS in stainless steel, copper, molybdenum and tantalum by applying even higher current densities that exceeded 1×10^{10} A/m^2. Lu et al. [21] also reported relaxation of RS in 1070 steel, but by using a pulsed magnetic field. In their work, they operated under conditions of what they termed "strong pulsed magnetic treatment," but did not define the value of the magnetic flux density. The results of numerical modelling from the present study show that the current density values during the treatment were significantly lower than the threshold level proposed by Baranov et al. [19]. These results suggest that in the present investigation, the induced eddy currents were not the main cause of RS relaxation.
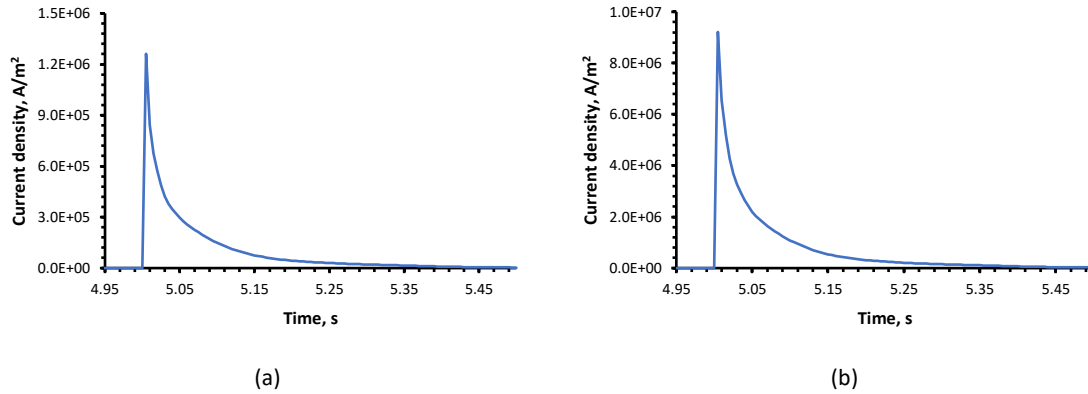
Figure 11. Eddy currents induced on the cylindrical surface of samples due to a change of magnetizing polarity; NAB (a) and AA2014-T6 (b).

The work of Molotskii [22] has provided the theoretical basis to suggest that the application of a magnetic field to a paramagnetic alloy (like AA2014) may trigger movement of dislocations. It is proposed that such motion is the result of the release of internal (residual) energy that accumulates in the material during manufacture. It was also suggested that the bonding energy of dislocation-to-paramagnetic obstacles (like impurities, vacancies, etc.) is dependent on the spin multiplicity of the radical pairs that are formed by the dislocation core and the obstacles. The radical pairs occur either in a singlet (with high binding energy) or in a triplet (with low binding energy) spin state. Application of a magnetic field may induce a transition from a singlet to a triplet state. As a consequence, the number of triplet states increases and weak coupling facilitates the unpinning of dislocations from obstacles. This stimulates dislocation movement due to the presence of a random field of long-range RS (stored internal energy). As AA2014-T6 is paramagnetic, the above-mentioned mechanism can explain the increase in the number of strengthening precipitates during the treatment. The alloy in the as-received state still contains some residual or "free" solute Cu in solution with aluminium. The application of the alternating magnetic field has caused an increase in the rate of diffusion of "free" solute Cu atoms to precipitate out of the solid solution to form GP zones and θ''. These changes can be referred to as secondary ageing [23] which is usually accompanied by increased strength of aluminium alloys.

The TEM and XRD analyses have shown changes in the microstructure of the NAB due to alternating magnetic field treatment. These changes are in the form of fewer and less tangled dislocations and more cuboidal κ_{IV} precipitates. The composition, morphology and crystal structure of the κ precipitates were recently studied by Wood [24] who has reported that the κ_{IV} precipitates (along with the precipitates κ_I, κ_{II} and κ_{Iii}) have an ordered crystal structure that is based on either Fe₃Al or NiAl. An investigation by Shull et al. [25] demonstrated the magnetic nature of Fe₃Al; according to Mitra [26], NiAl is also magnetic. Like all magnetic materials, these structural phases contain magnetic domains. When in the as-received state (without the application of the magnetic field), the magnetic moments of atoms in the NAB phases line up with one another, creating small domains oriented in random magnetisation directions. This situation is evident in Figure 12a, where randomly oriented domains in untreated NAB are presented schematically. Figure 12d presents an actual MFM scan of the untreated NAB (from the selected area shown in Figure 5a).

The application of an external magnetic field of 1.24 T causes rotation of the domains, yielding a higher magnetic flux density and magnetizing of NAB at levels up to 1.8 T. It can be suggested that at such levels of magnetic flux density, saturation will take place and the domains opposing the field will be swallowed up and disappear at least in some volume of the alloy with a high concentration of Fe₃Al and NiAl phases. A single-domain structure thus appears there as presented in Figure 12b. As reported by Chesnel [27], when the magnetic flux density approaches zero, the alternating polarity of the magnets will lead to changes in the magnetic domain pattern and to a gradual increase in the number of domains. On the other hand, when the applied magnetic field approaches its maximum value, a

decrease in the number of magnetic domains takes place. This alternating process continues throughout the treatment. The effect of the treatment is to minimise the internal energy of the material. This will involve a spontaneous division into separate magnetic domains with some final remanent domain pattern as shown in Figure 12c and Figure 12e. According to Celik et al. [28] and Wu et al. [29], the mobility of dislocations will increase substantially due to such domain wall movement. In addition, magnetostriction accompanying domain rotation induces micro-strains in the material. Altogether these factors can be the driving mechanism for the redistribution of dislocations in NAB to take place when alternating magnetic field treatment is applied. The process of domain rotation can be used to explain the behaviour of the κ_I, κ_{II} and κ_{III} phases, but the κ_{IV} precipitates exhibit significantly different behaviour due to their smaller size in comparison to the other precipitates. As shown in Figure 9b, most of the κ_{IV} precipitates have size ranging from about 10 nm to 30 nm. Within precipitates of this size range, magnetic particles have a single-domain state without magnetisation as reported by Binns [30] and they remain in this state for all applied magnetic fields [31, 32]. When in this state, they are characterised by high coercivity, therefore during reversing of the magnetisation of the κ_{IV} phase, the widest possible hysteresis loop for a particle of that composition is achieved. As a result, the largest possible work is performed on the material by the external field and this is dissipated as heat. This increased heating which is most likely localised around the κ_{IV} phase particles can promote extra diffusion mobility of "free" solute Fe and Al atoms to form more κ_{IV} (ie. Fe$_3$Al) precipitates from the retained β-phase and the α-phase.

Another possible mechanism that can promote diffusion mobility of solute Fe and small κ_{IV} phase particles is based on dipolar interaction which can cause an attraction or repulsion of magnetic dipoles. The energy levels of these interactions can be compared by considering a group of Fe atoms or single-domain κ_{IV} phase particles of the same size and magnetic moment, m. Let the distance between two atoms (particles) be r. When a magnetic field is applied, the magnetic moment of atoms or particles will be aligned along the field direction as presented in Figure 13a. According to Zhang et al. [33] and Cyrot [34], in this case the magnetic dipolar interaction energy, E_D, can be expressed as:

$$E_D = -\frac{\mu_0 m^2}{4\pi}\frac{3cos^2\theta - 1}{r^3}$$

where μ_0 is the vacuum magnetic permeability and θ is the angle between the vector r and the z-axis. This equation shows that the magnetic dipolar interaction energy, E_D, depends on the relative position of the interactive dipoles which is described by a geometric factor, f, where $f = \frac{3cos^2\theta-1}{r^3}$. Figure 13b presents the calculated values of the geometric factor as a function of the relative position of the dipoles.
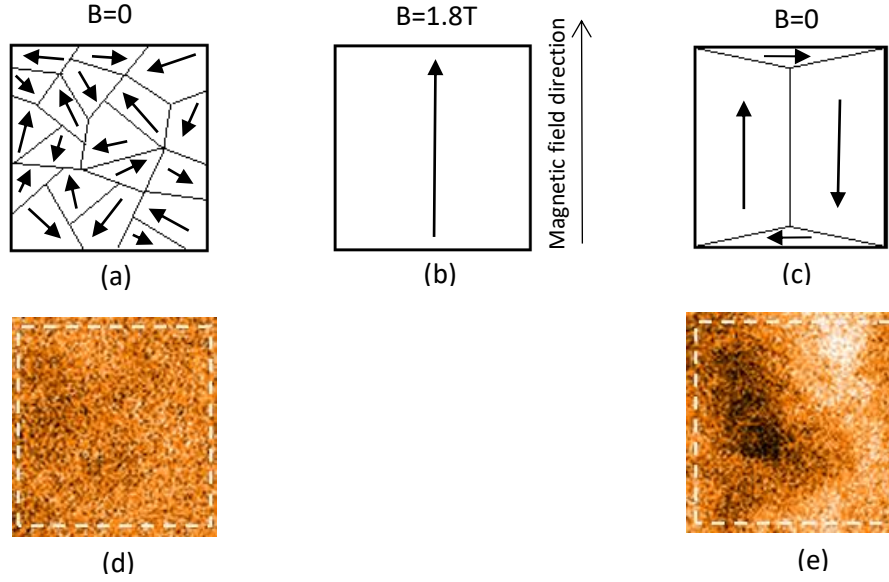
Figure 12. Domains and domain wall kinetics in tested samples; initial condition (a), after maximum magnetic field (saturation) (b), after treatment (c), fragment of MFM scan of sample in initial condition (see its location in Figure 7a) (d) and fragment of MFM scan of sample in condition after treatment (see its location in Figure 5b) (e).
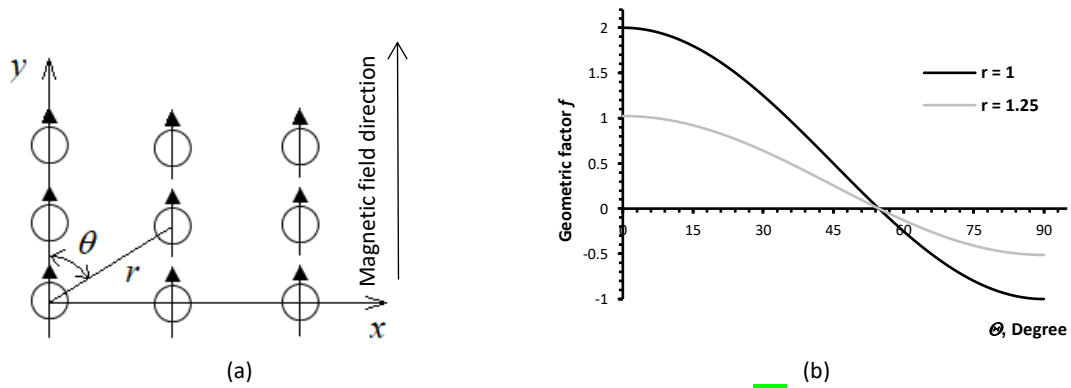

Figure 13. Alignment of Fe atoms or κ_{IV} single-domain dipoles under a magnetic field (a); variation of the geometrical factor f ,of the dipolar interaction energy E_D ,for $0 \le \Theta \le 90^0$ and for $r = 1$ and $r = 1.25$ (b).

From the calculated estimates of the geometrical factor, f, when two dipoles are parallel to the magnetic field direction, the magnetic dipolar interaction energy, E_D, is negative and the dipoles attract each other. On the other hand, when two dipoles are oriented perpendicular to the field direction, they repulse each other as the magnetic dipolar interaction energy, E_D, is positive. The maximum energy of attraction is two times higher than the maximum repulsive energy. Under this condition, the higher diffusion mobility of Fe atoms and Fe_3Al nuclei can facilitate the formation of more κ_{IV} precipitates.

Another source of κ_{IV} precipitates can be the eutectoid transformation of the β phase to the copper-rich α-phase plus κ eutectoid and further secondary κ precipitation based on Fe_3Al and NiAl. The XRD results in Figure 6 show that at $2\theta = 49.8^0$, there was a slight increase in the copper-rich α-phase as a result of the transformation of the β-phase to the α-phase and secondary κ precipitates (most probably κ_{IV}). The intensity of κ at $2\theta = 44.17^0$ increased only marginally and the peak has shifted slightly to the left (to a lower angle) after treatment. The width of this peak has also increased slightly as the shift (to the left) on the left-hand side of the peak is greater than the shift (to the left) on the right hand side of the peak. This suggests that the secondary κ_{IV} precipitates produced by the treatment have a slightly higher lattice parameter. Based on results of the effect of composition on

the lattice parameter of Fe_3Al as observed by Taylor and Jones [35], this change suggests that the secondary κ_{IV} may contain more iron and/or nickel.

The observed precipitation strengthening of both NAB and AA2014-T6 significantly improves the friction and wear of the two alloys. The reduction of tensile RS for the NAB alloy and the generation of compressive RS at the surface of the AA2014-T6 has benefited both alloys in terms of their tribological behaviour. These changes have taken place due to the increased mobility of dislocations as a result of alternating magnetic field treatment. The movement of dislocations towards the surface is more favourable since the external free surface of the samples can act as a natural sink for dislocations. Such movement is likely to create strain accumulation within the near-surface layer with a subsequent decrease of tensile RS in NAB and an increase of compressive RS in AA2014-T6.

As the research continues in order to gain better understanding of the mechanism leading to the effect of alternating magnetic field treatment, the possible influence of the induced eddy currents must not be dismissed entirely. Despite their relatively low amplitude ($1.26 \cdot 10^6$ A/m^2 for NAB and $9.2 \cdot 10^6$ A/m^2 for AA2014-T6) and their brief existence, eddy currents can create an additional back-force facilitating electromigration of both atoms and dislocations in metals to various equilibrium positions.

5. Conclusions

In this experimental study, the effect of alternating magnetic field treatment on the friction and wear resistance of NAB and AA2014-T6 aluminium alloy using AISI52100 steel ball bearing as the counter face material was investigated. Based on the results, the following conclusions can be drawn:

1. Both the coefficient of friction and the wear scar width of the two alloys were lower for the samples that had been treated by the alternating magnetic field.
2. Both alloys exhibited improved mechanical properties following alternating magnetic field treatment which led to an increase in the microhardness. XRD RS analysis revealed a decrease in tensile residual stresses in the near-surface layer of NAB and the formation of compressive residual stresses for the AA2014-T6 alloy following the treatment.
3. TEM examination showed that there was a reduction in the pile up of dislocations after treatment for both NAB and AA2014-T6 alloy. In both alloys, the treatment facilitated the generation of strengthening precipitates.
4. The precipitation mechanisms for the two alloys were different. For a paramagnetic material like AA2014-T6, the application of an alternating magnetic field can have an effect on the multiplicity of the radical pairs that are formed by the dislocation core. It can also facilitate such dislocation movement to bypass obstacles and can enable diffusion mobility of "free" solute Cu atoms in the aluminium matrix. In the case of the soft magnetic NAB, dislocation mobility and precipitation of the κ_{IV} phase after magnetic field treatment can be the result of domain rotation and dipolar interaction.

Acknowledgement

References

1. Bajwa, R., et al., *Wear and Friction Properties of Electrodeposited Ni-Based Coatings Subject to Nano-enhanced Lubricant and Composite Coating.* Acta Metallurgica Sinica (English Letters), 2016. **29**(10): p. 902-910.
2. Bockstedt, J. and B.E. Klamecki, *Effects of pulsed magnetic field on thrust bearing washer hardness.* Wear, 2007. **262**(9–10): p. 1086-1096.

3.   Bataineh, O., B. Klamecki, and B.G. Koepke, *Effect of pulsed magnetic treatment on drill wear.* Journal of Materials Processing Technology, 2003. **134**(2): p. 190-196.

4.   Babutskyi, A., A. Chrysanthou, and C. Zhao, *Effect of pulsed magnetic field pre-treatment of AISI 52100 steel on the coefficient of sliding friction and wear in pin-on-disk tests.* Friction, 2014. **2**(4): p. 310-316.

5.   Xi, X., Y. Xia, and Y. Hu, *The Effects of Magnetic Treatment on the Tribological Behavior of AISI 1045 Steel under Lubricated Conditions.* Tribology Transactions, 2018. **61**(4): p. 671-682.

6.   Richardson, I., *Guide to nickel aluminium bronze for engineers*. 2016: Copper Development Association.

7.   Lall, C., et al., *Wear Resistance and Mechanical Properties of Selected PM Aluminum Alloys and Composites.* Advances in Powder Metallurgy and Particulate Materials, 2013: p. 1-17.

8.   Astm, G., *99–95a Standard Test Method for Wear Testing with a Pin-on-Disk Apparatus.* ASTM International, 2000.

9.   Bhaumik, S. and S.D. Pathak, *A Comparative Experimental Analysis of Tribological Properties Between Commercial Mineral Oil and Neat Castor Oil using Taguchi Method in Boundary Lubrication Regime.* Tribology in Industry, 2016. **38**: p. 33-44.

10.   Tariq, F., et al., *Characterization of Material Properties of 2xxx Series Al-Alloys by Non Destructive Testing Techniques.* Journal of Nondestructive Evaluation, 2012. **31**(1): p. 17-33.

11.   Lourdjane, F. and A.A. Raho, *Precipitation Kinetics of the GP Zones in Al4,65at.% Ag(15%Wt.).* American Journal of Materials Science and Engineering, 2015. **3**(1): p. 11-14.

12.   Refaey, A.A., M. Abdel-Rahman, and E.A. Badawi. *Artificial ageing effect on mechanical, electrical properties and positron lifetime of aircraft 2024 alloy*. in *Defect and Diffusion Forum*. 2012. Trans Tech Publ.

13.   Prabhu, T.R., *Effects of ageing time on the mechanical and conductivity properties for various round bar diameters of AA 2219 Al alloy.* Engineering Science and Technology, an International Journal, 2017. **20**(1): p. 133-142.

14.   Popović, M. and E. Romhanji, *Characterization of microstructural changes in an Al-6.8 wt.% Mg alloy by electrical resistivity measurements.* Materials Science and Engineering: A, 2008. **492**(1-2): p. 460-467.

15.   Cseh, D. and V. Mertinger, *X-Ray Diffraction Measurements of Residual Stress Induced by Surface Compressing Methods*. Vol. 729. 2012. 199-204.

16.   Akram, S., et al., *Effect of Alternating Magnetic Field on the Fatigue Behaviour of EN8 Steel and 2014-T6 Aluminium Alloy.* Metals, 2019. **9**(9): p. 984.

17.   Tang, G., et al., *Effect of a pulsed magnetic treatment on the dislocation substructure of a commercial high strength steel.* Materials Science and Engineering: A, 2005. **398**(1–2): p. 108-112.

18.   Magweb, *Free BH Curves - Magweb.* Magweb.

19.   Baranov, Y.V., et al., *Physical bases of electric-pulse and electroplastic treatments and new materials.* Chap, 2001. **1**: p. 56-77.

20.   Stepanov, G.V., et al., *Analysis of pulse current-induced tensile stress relaxation.* Strength of Materials, 2006. **38**(1): p. 84-91.

21.   Lu, A.L., et al., *Research on residual-stress reduction by strong pulsed magnetic treatment.* Journal of Materials Processing Technology, 1998. **74**(1–3): p. 259-262.

22.   Molotskii, M.I., *Theoretical basis for electro-and magnetoplasticity.* Materials Science and Engineering: A, 2000. **287**(2): p. 248-258.

23.   Polmear, I., *Light alloys: from traditional alloys to nanocrystals*. 2005: Elsevier.

24.   Wood, R.J., *Marine wear and tribocorrosion.* Wear, 2017. **376**: p. 893-910.

25.   Shull, R.D., H. Okamoto, and P.A. Beck, *Transition from ferromagnetism to mictomagnetism in Fe—Al alloys.* Solid State Communications, 1976. **20**(9): p. 863-868.

26.   Mitra, R., *Intermetallic Matrix Composites: Properties and Applications*. 2017: Elsevier.

27. Chesnel, K., *Nanoscale Magnetic Domain Memory*, in *Magnetism and Magnetic Materials*. 2017, IntechOpen.

28. Çelik, A., et al., *Effect of magnetic treatment on fatigue life of AISI 4140 steel.* Materials & Design, 2005. **26**(8): p. 700-704.

29. Wu, S., et al., *A micro-mechanism model of residual stress reduction by low frequency alternating magnetic field treatment.* Journal of Materials Processing Technology, 2003. **132**(1): p. 198-202.

30. Binns, C., *Introduction to nanoscience and nanotechnology*. Vol. 14. 2010: John Wiley & Sons.

31. Stoner, E.C. and E. Wohlfarth, *A mechanism of magnetic hysteresis in heterogeneous alloys.* Philosophical Transactions of the Royal Society of London. Series A, Mathematical and Physical Sciences, 1948. **240**(826): p. 599-642.

32. Wohlfarth, E., *Hard magnetic materials.* Advances in physics, 1959. **8**(30): p. 87-224.

33. Zhang, Y., et al., *Grain boundary characteristics and texture formation in a medium carbon steel during its austenitic decomposition in a high magnetic field.* Acta materialia, 2005. **53**(19): p. 5213-5221.

34. Cyrot, M., *Magnetisme.* Grenoble: Presses Universitaires de Grenoble, 1999: p. p. 37, 65

35. Taylor, A. and R.M. Jones, *Constitution and magnetic properties of iron-rich iron-aluminum alloys.* Journal of Physics and Chemistry of Solids, 1958. **6**(1): p. 16-37.